



INFLUENCE OF UNIAXIAL AND HYDROSTATIC PRESSURES AND A LONGITUDINAL ELECTRIC FIELD ON THE THERMODYNAMIC CHARACTERISTICS OF THE QUASI-ONE-DIMENSIONAL FERROELECTRIC CsH_2PO_4

A. S. Vdovych¹ , R. R. Levitskii¹, I. R. Zachek², A. P. Moina¹ 

¹*Institute for Condensed Matter Physics of the National Academy of Sciences of Ukraine,
1, Svientsitskii St., Lviv, UA-79011, Ukraine,*

²*Lviv Polytechnic National University,
12, Bandery St., Lviv, UA-79013, Ukraine*

(Received 04 January 2021; in final form 22 April 2021; accepted 11 May 2021; published online 14 July 2021)

We propose a two-sublattice proton ordering model for the quasi-one-dimensional CsH_2PO_4 ferroelectric with hydrogen bonds, which takes into account contributions to the energy of the proton subsystem that are linear in the lattice strains ε_1 , ε_2 , ε_3 , and ε_5 . The model also takes into account the dependence of the effective dipole moments of pseudospins on the order parameters, which enables us to coordinate the values of the effective dipole moments in the paraelectric and ferroelectric phases. Within this model in the two-particle cluster approximation for the short-range interactions and in the mean field approximation for the long-range interactions, the behavior of spontaneous polarization, longitudinal dielectric permittivity, piezoelectric and elastic characteristics, and molar heat capacity under the influence of uniaxial and hydrostatic pressure and a longitudinal electric field are investigated.

Key words: ferroelectrics, dielectric permittivity, piezoelectric coefficients, pressure effect, electric field effect.

DOI: <https://doi.org/10.30970/jps.25.3702>

I. INTRODUCTION

Investigations of the external pressure and field effects in ferroelectrics are an important problem of ferroelectrics physics. High pressure studies give a possibility to obtain additional valuable information on the peculiarities of the behavior of the physical properties of ferroelectric compounds, as well as to search for new physical effects, which are not observed under zero pressure and zero external field. It should be also underlined that these studies give an opportunity to understand

better the mechanisms of phase transitions in these materials.

The ferroelectric with hydrogen bonds CsH_2PO_4 (CDP) is an example of a crystal, where the pressure and field effects are essential. In this crystal, there are two structurally non-equivalent types of hydrogen bonds of different lengths (Fig. 1,b). The longer bonds have one equilibrium position for protons, whereas the shorter bonds have two equilibrium positions. They link PO_4 groups into chains along the b -axis (Fig. 1,a); therefore the crystal is quasi-one-dimensional.

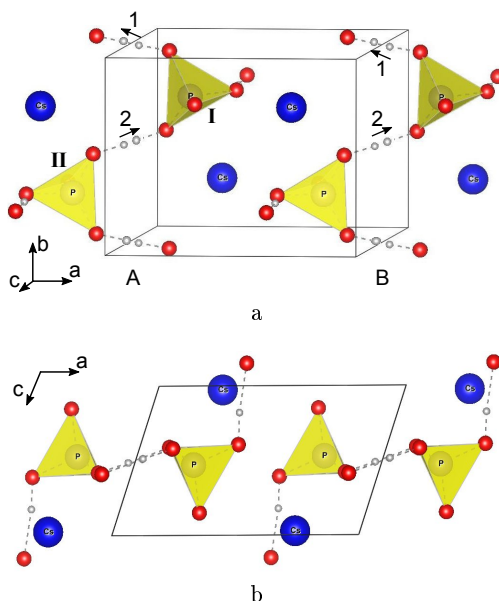


Fig. 1. The primitive cell of the CsH_2PO_4 crystal in the ferroelectric phase

At room temperature and zero pressure, the crystal is in the paraelectric phase and has a monoclinic symmetry (the space group $P2_1/m$) [1, 2]. Protons on the shorter bonds occupy two equilibrium positions with equal probability. Below $T_c = 153$ K, the crystal goes into the ferroelectric phase (the space group $P2_1$) [3, 4] with spontaneous polarization along the crystallographic b -axis, and the protons occupy mainly upper equilibrium positions (Fig. 1, a).

On the basis of dielectric measurements [5, 6] it was determined that under pressure $p_c = 0.33$ GPa and $T_c^{\text{cr}} = 124.6$ K there appear double hysteresis loops, that is, the crystal goes to the antiferroelectric phase. By neutron scattering experiments [7] it has been established that in the antiferroelectric phase the primitive cell of CDP crystal doubles along the a -axis, because there appear two sublattices in the form of bc -planes, which are polarized antiparallelly along the b -axis and alternate along the a -axis. The symmetry of the crystal remains monoclinic (the space group $P2_1$), and the constants of the double lattice are as follows: $a = 15.625$ Å, $b = 6.254$ Å, $c = 4.886$ Å, $\beta = 108.08^\circ$. A significant shift of Cs atoms and PO_4 groups in (a, c) -plane and rotation of the PO_4 groups by 36.8° around the b -axis, which goes through the P atom, occur. The protons on the hydrogen bonds of neighboring sublattices are ordered antiparallelly. At very high pressures, the antiferroelectric phase of a second type (AF2) appears, where two sublattices have a form of chains along the b -axis, which are polarized antiparallelly along b -axis and have a checkerboard arrangement. The AF2 phase was predicted in [8] on the basis of NMR data [8] and confirmed in [9] on the basis of dielectric constant measurements at low temperature and X-ray diffraction experiments.

Influence of hydrostatic pressure on the transition temperature in the $\text{Cs}(\text{H}_{1-x}\text{D}_x)_2\text{PO}_4$ ferroelectrics was explored in [5, 6, 9–12].

Results of experimental measurements of the temperature dependence of spontaneous polarization of the CsH_2PO_4 crystal at different values of hydrostatic pressure are presented in [6], and of the static longitudinal dielectric permittivity in [6, 9, 11, 12].

The lattice dynamics of CsH_2PO_4 and CsD_2PO_4 crystals was explored in [13, 14]. The phonon spectra of these crystals and specific heat were calculated. The obtained temperature variation of the specific heat qualitatively agrees with the experimental data, except for the vicinity of the phase transition. Later, the ab initio calculations have shown an important role of proton tunneling [15], and also the piezoelectric coefficients, elastic constants, and specific heat of CsH_2PO_4 [16, 17].

An attempt to theoretically describe the paraelectric-ferroelectric and paraelectric-antiferroelectric phase transition in CsH_2PO_4 and CsD_2PO_4 as well as experimental data for the dielectric permittivity was done in [18], where the crystal was described as pseudospin Ising chains. However, the description of the experimental data for the dielectric constant by the proposed theory was not considered.

Later [19], using the pseudospin model [18] and

the two-particle cluster approximation for the short-range configuration interactions, the thermodynamic and dynamic characteristics of CDP type ferroelectrics were calculated at different values of hydrostatic pressure. A good agreement of the theory with the experimental data for the dielectric constant and for the pressure dependence of the para-ferroelectric and para-antiferroelectric phase transition temperatures was obtained. However, in the model [18, 19] one cannot calculate the piezoelectric and elastic characteristics of the crystal, and the critical pressure does not depend on temperature.

In [20], the temperature dependences of the lattice strains $\varepsilon_1, \varepsilon_2, \varepsilon_3, \varepsilon_5$ were measured. There was also proposed a quasi-one-dimensional Ising model for the CsH_2PO_4 crystal, where the interaction parameters were linear functions of these strains. On the basis of this model, the temperature dependences of $\varepsilon_j(T)$ were explained. However, this model does not consider the crystal as two sublattices and does not allow one to describe the ferroelectric-antiferroelectric phase transition under high pressures.

In [21], a two-sublattice model of a deformed CsH_2PO_4 crystal has been proposed, where the interactions between neighboring pseudospins within a chain are taken into account in the two-particle cluster approximation, whereas the long-range interactions (including the interchain ones) are considered in the mean field approximation. The interaction parameters are taken to be linear functions of the strains ε_j . As a result, the temperature dependences of spontaneous polarization, dielectric permittivity, piezoelectric coefficients, and elastic constants were calculated.

In [22], using the model of the deformed CsH_2PO_4 crystal, proposed in [21] the effects of hydrostatic pressure on the phase transition temperature, longitudinal static dielectric characteristics of $\text{Cs}(\text{H}_{1-x}\text{D}_x)_2\text{PO}_4$ crystals were studied.

As is well known, in the presence of the longitudinal field E_y , the second order phase transition is smeared, and the temperature dependence of the longitudinal permittivity $\varepsilon_{yy}(T)$ has a rounded maximum. At the same time, in [21, 22], to calculate the longitudinal dielectric permittivity ε_{yy} , different values for the effective dipole moments in the paraelectric and ferroelectric phases were used. This gives rise to a jump in the $\varepsilon_{yy}(T)$ curve, instead of the rounded maximum expected in presence of the external field E_y . Therefore, in order to describe the smearing of phase transition, in [23] we have modified the model [21] by assuming that the effective dipole moment on a hydrogen bond depends on the order parameter on this bond, because the order parameter depends on temperature continuously near the phase transition point. The behavior of spontaneous polarization, longitudinal dielectric permittivity, and molar specific heat in the presence of hydrostatic pressure and a longitudinal electric field was explored [23].

In the present paper, we study the behavior of the spontaneous polarization, longitudinal dielectric permittivity, piezoelectric and elastic characteristics, and

molar specific heat of CsH_2PO_4 in the presence of uniaxial and hydrostatic pressure, a longitudinal electric field, considering also the case when the pressures and the electric field are applied simultaneously.

II. THE MODEL OF THE CsH_2PO_4 CRYSTAL

We study the system of protons in the CsH_2PO_4 crystal, moving on the short $\text{O-H}\dots\text{O}$ bonds between the HPO_4 groups, which form zigzag chains along the crystallographic b -axis of the crystal (see Fig.1).

The cell contains one chain, marked as “A” in Fig. 1. In order to describe the transition to the antiferroelectric phase, under high pressure we shall consider an extended primitive cell, which includes two chains (“A” and “B”). All the “A” chains form the sublattice “A”, whereas all the “B” chains form the sublattice “B”. Every chain in the

primitive cell includes two neighboring PO_4 tetrahedra (of type “I” and “II”) together with two short hydrogen bonds (respectively, “1” and “2”).

Let us ascribe the dipole moments $\mathbf{d}_{q1}^A, \mathbf{d}_{q2}^A, \mathbf{d}_{q1}^B, \mathbf{d}_{q2}^B$ to the protons on the bonds. The pseudospin variables $\frac{\sigma_{q1}^A}{2}, \frac{\sigma_{q2}^A}{2}, \frac{\sigma_{q1}^B}{2}, \frac{\sigma_{q2}^B}{2}$ describe the changes associated with reordering of the respective dipole moments of the structure units: $\mathbf{d}_{q1,2}^{A,B} = \mu \frac{\sigma_{q1,2}^{A,B}}{2}$. The mean values $\langle \frac{\sigma}{2} \rangle = \frac{1}{2}(n_a - n_b)$ are related to the differences in occupancies of the two possible positions or the protons on the bonds, n_a and n_b .

The Hamiltonian of the proton subsystem of CsH_2PO_4 takes into account the short-range and long-range interactions. Under the stresses maintaining the symmetry of crystal $\sigma_1 = \sigma_{xx}, \sigma_2 = \sigma_{yy}, \sigma_3 = \sigma_{zz}, \sigma_5 = \sigma_{xz}$ ($X \perp (b,c), Y \parallel b, Z \parallel c$), and in the presence of electric field $E_2 = E_y$, it can be written as [23]:

$$\begin{aligned} \hat{H} = & Nv \left\{ \frac{1}{2} \sum_{j,j'} c_{jj'}^{E0} \varepsilon_j \varepsilon_{j'} - \sum_j e_{2j}^0 E_2 \varepsilon_j - \frac{1}{2} \chi_{22}^{E0} E_2^2 \right\} \\ & - 2w \sum_{qq'} \left(\frac{\sigma_{q1}^A}{2} \frac{\sigma_{q'2}^A}{2} + \frac{\sigma_{q1}^B}{2} \frac{\sigma_{q'2}^B}{2} \right) (\delta_{\mathbf{R}_q \mathbf{R}_{q'}} + \delta_{\mathbf{R}_q + \mathbf{R}_b, \mathbf{R}_{q'}}) \\ & + \hat{H}_{\text{long}} - \sum_q \mu_y E_2 \left(\frac{\sigma_{q1}^A}{2} + \frac{\sigma_{q2}^A}{2} + \frac{\sigma_{q1}^B}{2} + \frac{\sigma_{q2}^B}{2} \right) \\ & - 3 \left\{ \sum_q \left(\frac{\eta_1^2 \sigma_{q1}^A}{2} + \frac{\eta_1^2 \sigma_{q2}^A}{2} + \frac{\eta_2^2 \sigma_{q1}^B}{2} + \frac{\eta_2^2 \sigma_{q2}^B}{2} \right) + 2N(\eta_1^3 + \eta_2^3) \right\} \mu' E_2, \end{aligned} \quad (2.1)$$

where N is the total number of extended primitive cells of the Bravais lattice; v is their volume.

The first term in (2.1) is the “seed” energy, which corresponds to the heavy ion sublattice and does not explicitly depend on the configuration of the proton subsystem. It includes the elastic, piezoelectric, and dielectric parts, expressed in terms of the electric field E_2 , and strains preserving the symmetry of the crystal $\varepsilon_1 = \varepsilon_{xx}, \varepsilon_2 = \varepsilon_{yy}, \varepsilon_3 = \varepsilon_{zz}, \varepsilon_5 = 2\varepsilon_{xz}$. $c_{jj'}^{E0}, e_{2j}^0, \chi_{22}^{E0}$ ($j=1,2,3,5$) are the “seed” elastic constants, coefficients of piezoelectric stress, and dielectric susceptibility of a mechanically clamped crystal.

The second term in (2.1) is the Hamiltonian of the short-range interactions. In (2.1), $\sigma_{q1,2}^{A,B}$ are the z -components of the pseudospin operator that describe the state of the bond “1” or “2” of the chain “A” or “B”, in the q -th cell, \mathbf{R}_b is the lattice vector along the OY -axis. The first and the second Kronecker delta-symbols correspond to the interaction between protons in the chains near the

tetrahedra PO_4 of type “I” and of type “II”, respectively. The contributions to the energy of interactions between pseudospins near tetrahedra of different types are identical.

The parameter w , which describes the short-range interactions within the chains, is expanded linearly into a series over the strains ε_j

$$w = w^0 + \sum_j \delta_{2j} \varepsilon_j, \quad j = 1, 2, 3, 5. \quad (2.2)$$

The term \hat{H}_{long} in (2.1) describes the long-range dipole-dipole interactions and indirect (via the lattice vibrations) interactions between protons, taken into account in the mean field approximation

$$\hat{H}_{\text{long}} = NH^0 + \hat{H}_2, \quad (2.3)$$

where

$$\begin{aligned}
H^0 = & \frac{1}{8} \left[J_{11} \left(\langle \sigma_1^A \rangle^2 + \langle \sigma_1^B \rangle^2 \right) + J_{22} \left(\langle \sigma_2^A \rangle^2 + \langle \sigma_2^B \rangle^2 \right) + 2J_{12} \left(\langle \sigma_1^A \rangle \langle \sigma_2^A \rangle + \langle \sigma_1^B \rangle \langle \sigma_2^B \rangle \right) \right] \\
& + \frac{1}{4} \left[K_{11} \left(\sigma_1^A \langle \sigma_1^B \rangle \right) + K_{22} \left(\sigma_2^A \langle \sigma_2^B \rangle \right) + K_{12} \left(\langle \sigma_1^A \rangle \langle \sigma_2^B \rangle + \langle \sigma_1^B \rangle \langle \sigma_2^A \rangle \right) \right], \quad (2.4)
\end{aligned}$$

$$\begin{aligned}
\hat{H}_2 = & - \sum_q \left\{ \left(J_{11} \langle \sigma_1^A \rangle + J_{12} \langle \sigma_2^A \rangle + K_{11} \langle \sigma_1^B \rangle + K_{12} \langle \sigma_2^B \rangle \right) \frac{\sigma_{q1}^A}{4} + \left(J_{12} \langle \sigma_1^A \rangle + J_{22} \langle \sigma_2^A \rangle + K_{12} \langle \sigma_1^B \rangle + K_{22} \langle \sigma_2^B \rangle \right) \frac{\sigma_{q2}^A}{4} \right. \\
& + \left. \left(J_{11} \langle \sigma_1^B \rangle + J_{12} \langle \sigma_2^B \rangle + K_{11} \langle \sigma_1^A \rangle + K_{12} \langle \sigma_2^A \rangle \right) \frac{\sigma_{q1}^B}{4} + \left(J_{12} \langle \sigma_1^B \rangle + J_{22} \langle \sigma_2^B \rangle + K_{12} \langle \sigma_1^A \rangle + K_{22} \langle \sigma_2^A \rangle \right) \frac{\sigma_{q2}^B}{4} \right\}. \quad (2.5)
\end{aligned}$$

Here the parameters $J_{ff'} = \sum_{\mathbf{R}_q - \mathbf{R}_{q'}} J_{ff'}(qq')$ and $K_{ff'} =$

$\sum_{\mathbf{R}_q - \mathbf{R}_{q'}} K_{ff'}(qq')$ are the Fourier transforms of the long-range interaction constants at $\mathbf{k} = 0$.

Let us expand the parameters $J_{ff'}$ i $K_{ff'}$ in series over the strains ε_j up to the linear terms

$$J_{11} = J_{22} = J_1 + \sum_j \bar{\varphi}_{1j} \varepsilon_j,$$

$$J_{12} = J_{21} = J_2 + \sum_j \bar{\varphi}_{2j} \varepsilon_j,$$

$$K_{11} = K_{22} = K_1 + \sum_j \varphi_{1j} \varepsilon_j,$$

$$K_{12} = K_{21} = K_2 + \sum_j \varphi_{2j} \varepsilon_j.$$

Taking into account the following symmetry of pseudospins in the chains

$$\langle \sigma_{q1}^A \rangle = \langle \sigma_{q2}^A \rangle = \eta_1, \quad \langle \sigma_{q1}^B \rangle = \langle \sigma_{q2}^B \rangle = \eta_2 \quad (2.6)$$

we obtain the expressions for (2.4), (2.5) as

$$\hat{H}^0 = \nu_1 (\eta_1^2 + \eta_2^2) + 2\nu_2 \eta_1 \eta_2, \quad (2.7)$$

$$\begin{aligned}
\hat{H}_2 = & \sum_q \left\{ - (2\nu_1 \eta_1 + 2\nu_2 \eta_2) \left(\frac{\sigma_{q1}^A}{2} + \frac{\sigma_{q2}^A}{2} \right) \right. \\
& - \left. (2\nu_2 \eta_1 + 2\nu_1 \eta_2) \left(\frac{\sigma_{q1}^B}{2} + \frac{\sigma_{q2}^B}{2} \right) \right\}. \quad (2.8)
\end{aligned}$$

Here we used the following notations

$$\begin{aligned}
\nu_1 = & \frac{1}{8} (J_{11} + J_{22} + 2J_{12}) = \nu_1^0 + \sum_j \psi_{j1} \varepsilon_j, \\
\nu_1^0 = & \frac{1}{4} (J_1 + J_2), \quad \psi_{j1} = \frac{1}{4} (\bar{\varphi}_{1j} + \varphi_{1j}), \quad (2.9)
\end{aligned}$$

$$\begin{aligned}
\nu_2 = & \frac{1}{8} (K_{11} + K_{22} + 2K_{12}) = \nu_2^0 + \sum_j \psi_{j2} \varepsilon_j, \\
\nu_2^0 = & \frac{1}{4} (K_1 + K_2), \quad \psi_{j2} = \frac{1}{4} (\bar{\varphi}_{2j} + \varphi_{2j}). \quad (2.10)
\end{aligned}$$

The fourth term in (2.1) describes the interactions of pseudospins with the external electric field, whereas the term \hat{H}'_E takes into account the abovementioned dependence of effective dipole moments on the mean value of pseudospin s_f

The two-particle cluster approximation for short-range interactions is used to calculate the thermodynamic characteristics of CDP. In this approximation, the thermodynamic potential is given by

$$\begin{aligned}
G = & NU_{\text{seed}} + NH^0 + 2N(\eta_1^3 + \eta_2^3) \mu' E_2 - Nv \sum_j \sigma_j \varepsilon_j \\
& - k_B T \sum_q \left\{ 2 \ln \text{Sp} e^{-\beta \hat{H}_q^{(2)}} - \ln \text{Sp} e^{-\beta \hat{H}_q^{(1)A}} - \ln \text{Sp} e^{-\beta \hat{H}_q^{(1)B}} \right\}, \quad (2.11)
\end{aligned}$$

where $\beta = \frac{1}{k_B T}$, k_B is the Boltzmann constant; $\hat{H}_q^{(2)}$, $\hat{H}_q^{(1)A}$, $\hat{H}_q^{(1)B}$ are two-particle and one-particle Hamiltonians

given by

$$\hat{H}_q^{(2)} = -2w \left(\frac{\sigma_{q1}^A \sigma_{q2}^A}{2} + \frac{\sigma_{q1}^B \sigma_{q2}^B}{2} \right) - \frac{y_1}{\beta} \left(\frac{\sigma_{q1}^A}{2} + \frac{\sigma_{q2}^A}{2} \right) - \frac{y_2}{\beta} \left(\frac{\sigma_{q1}^B}{2} + \frac{\sigma_{q2}^B}{2} \right), \quad (2.12)$$

$$\hat{H}_q^{(1)A} = -\frac{\bar{y}_1}{\beta} \left(\frac{\sigma_{q1}^A}{2} + \frac{\sigma_{q2}^A}{2} \right), \quad \hat{H}_q^{(1)B} = -\frac{\bar{y}_2}{\beta} \left(\frac{\sigma_{q1}^B}{2} + \frac{\sigma_{q2}^B}{2} \right), \quad (2.13)$$

where the following notations are used

$$y_1 = \beta \Delta_1 + 2\beta \nu_1 \eta_1 + 2\beta \nu_2 \eta_2 + \beta(\mu_y E_2 + 3\eta_1^2 \mu' E_2), \quad (2.14)$$

$$y_2 = \beta \Delta_2 + 2\beta \nu_2 \eta_1 + 2\beta \nu_1 \eta_2 + \beta(\mu_y E_2 + 3\eta_2^2 \mu' E_2), \quad (2.15)$$

$$\bar{y}_1 = \beta \Delta_1 + y_1, \quad \bar{y}_2 = \beta \Delta_2 + y_2.$$

Here Δ_l are the effective fields created by the neighboring bonds from outside the cluster. In the cluster approximation, these fields can be determined from the condition of the minimum of thermodynamic potential $\partial G / \partial \Delta_l = 0$, yielding the self-consistency condition, which states that the mean values of the pseudospins $\langle \sigma_{qf}^{A,B} \rangle$ calculated using two-particle and one-particle Gibbs distributions should coincide

$$\eta_1 = \frac{\text{Sp} \sigma_{qf}^A e^{-\beta \hat{H}_q^{(2)}}}{\text{Sp} e^{-\beta \hat{H}_q^{(2)}}} = \frac{\text{Sp} \sigma_{qf}^A e^{-\beta \hat{H}_q^{(1)A}}}{\text{Sp} e^{-\beta \hat{H}_q^{(1)A}}},$$

$$\eta_2 = \frac{\text{Sp} \sigma_{qf}^B e^{-\beta \hat{H}_q^{(2)}}}{\text{Sp} e^{-\beta \hat{H}_q^{(2)}}} = \frac{\text{Sp} \sigma_{qf}^B e^{-\beta \hat{H}_q^{(1)B}}}{\text{Sp} e^{-\beta \hat{H}_q^{(1)B}}}. \quad (2.16)$$

Hence, on the basis (2.16) with taking into account of (2.6), (2.12) and (2.13), we obtain the expressions for the order parameters

$$\begin{aligned} \eta_1 &= \frac{1}{D} [\sinh(y_1 + y_2) + \sinh(y_1 - y_2) + 2a \sinh y_1] \\ &= \tanh \frac{\bar{y}_1}{2}, \\ \eta_2 &= \frac{1}{D} [\sinh(y_1 + y_2) - \sinh(y_1 - y_2) + 2a \sinh y_2] \\ &= \tanh \frac{\bar{y}_2}{2}, \end{aligned} \quad (2.17)$$

where the following notations are used

$$D = \cosh(y_1 + y_2) + \cosh(y_1 - y_2) + 2a \cosh y_1 + 2a \cosh y_2 + 2a^2,$$

$$a = e^{-\frac{v}{k_B T}}.$$

Excluding the cluster fields Δ_l from the expression $\eta_l = \tanh(\bar{y}_l/2)$ (see (2.17)), we write down (2.14), (2.15) as

$$y_1 = \frac{1}{2} \ln \frac{1 + \eta_1}{1 - \eta_1} + \beta \nu_1 \eta_1 + \beta \nu_2 \eta_2 + \frac{1}{2} \beta (\mu_y E_2 + 3\eta_1^2 \mu' E_2),$$

$$y_2 = \frac{1}{2} \ln \frac{1 + \eta_2}{1 - \eta_2} + \beta \nu_2 \eta_1 + \beta \nu_1 \eta_2 + \frac{1}{2} \beta (\mu_y E_2 + 3\eta_2^2 \mu' E_2).$$

III. THE STATIC LONGITUDINAL DIELECTRIC, PIEZOELECTRIC, ELASTIC, AND THERMAL CHARACTERISTICS OF CDP

Using (2.11), we write the thermodynamic potential per one extended primitive cell as

$$g = U_{\text{seed}} + H^0 + 2(\eta_1^3 + \eta_2^3) \mu' E_2 + 2k_B T \ln 2 - 2w - v \sum_j \sigma_j \varepsilon_j$$

$$- k_B T \ln(1 - \eta_1^2) - k_B T \ln(1 - \eta_2^2) - 2k_B T \ln D. \quad (3.1)$$

Using the equilibrium condition

$$\left(\frac{\partial g}{\partial \varepsilon_j} \right)_{E_2} = 0,$$

we obtain a set of equations for the strains ε_j :

$$\sigma_j = c_{j1}^{E0} \varepsilon_1 + c_{j2}^{E0} \varepsilon_2 + c_{j3}^{E0} \varepsilon_3 + c_{j5}^{E0} \varepsilon_5 - e_{2j}^0 E_2 - \frac{2\delta_j}{v} + \frac{4\delta_j}{vD} M - \frac{1}{v} \psi_{j1} (\eta_1^2 + \eta_2^2) - \frac{2}{v} \psi_{j2} \eta_1 \eta_2, \quad (3.2)$$

where

$$M = [a \cosh y_1 + a \cosh y_2 + 2a^2].$$

For hydrostatic pressure, the stresses in (3.2) are $\sigma_1 = \sigma_2 = \sigma_3 = -p_h$, $\sigma_5 = 0$. For the uniaxial stresses applied along the axis a , $\sigma_1 = -p_1$, $\sigma_2 = \sigma_3 = \sigma_5 = 0$, along the axis b , $\sigma_2 = -p_2$, $\sigma_1 = \sigma_3 = \sigma_5 = 0$, along the axis c , $\sigma_3 = -p_3$, $\sigma_1 = \sigma_2 = \sigma_5 = 0$. Hence we obtained the set of equations (2.17), (3.2) for the order parameters η_f and strains $\varepsilon_i, \varepsilon_5$.

On the basis of thermodynamic potential (3.1) we easily obtain expressions for different thermodynamic characteristics. In particular, the expression for longitudinal polarization P_2 reads

$$P_2 = - \left(\frac{\partial g}{\partial E_2} \right)_{\sigma_i} = \sum_j e_{2j}^0 \varepsilon_j + \chi_{22}^{E0} E_2 + \frac{\mu_y}{v} (\eta_1 + \eta_2) + \frac{\mu'}{v} (\eta_1^3 + \eta_2^3). \quad (3.3)$$

The isothermal static dielectric susceptibility of a mechanically clamped crystal is

$$\begin{aligned} \chi_{22}^{E0} &= \left(\frac{\partial P_2}{\partial E_2} \right)_{\varepsilon_i} = \chi_{22}^{E0} + \frac{\beta \tilde{\mu}_{1y}^2}{2v\Delta} \{ D(\kappa_{11} + \kappa_{12}(\tilde{\varphi}_2 - \beta\nu_2)(\kappa_{11}\kappa_{22} - \kappa_{12}^2)) \} \\ &+ \frac{\beta \tilde{\mu}_{2y}^2}{2v\Delta} \{ D(\kappa_{12} + \kappa_{22}) - (\tilde{\varphi}_1 - \beta\nu_2)(\kappa_{11}\kappa_{22} - \kappa_{12}^2) \}, \end{aligned} \quad (3.4)$$

where the following notations are used

$$\begin{aligned} \Delta &= D^2 - D[\tilde{\varphi}_1 \kappa_{11} + \tilde{\varphi}_2 \kappa_{22} + 2\beta\nu_2 \kappa_{12}] + [\tilde{\varphi}_1 \tilde{\varphi}_2 - (\beta\nu_2)^2](\kappa_{11}\kappa_{22} - \kappa_{12}^2), \\ \tilde{\varphi}_1 &= \varphi_1 + 3\eta_1 \beta \mu' E_2, \quad \tilde{\varphi}_2 = \varphi_2 + 3\eta_2 \beta \mu' E_2, \\ \varphi_1 &= \frac{1}{1 - \eta_1^2} + \beta\nu_1, \quad \varphi_2 = \frac{1}{1 - \eta_2^2} + \beta\nu_1, \\ \tilde{\mu}_{1y} &= \mu_y + 3\mu' \eta_1^2, \quad \tilde{\mu}_{2y} = \mu_y + 3\mu' \eta_2^2, \\ \kappa_{11} &= \cosh(y_1 + y_2) + \cosh(y_1 - y_2) + 2a \cosh y_1 - \eta_1^2 D, \\ \kappa_{12} &= \cosh(y_1 + y_2) - \cosh(y_1 - y_2) - \eta_1 \eta_2 D, \\ \kappa_{22} &= \cosh(y_1 + y_2) + \cosh(y_1 - y_2) + 2a \cosh y_2 - \eta_2^2 D. \end{aligned}$$

The isothermal coefficients of piezoelectric stress are

$$e_{2l} = \left(\frac{\partial P_2}{\partial \varepsilon_l} \right)_{E_2} = e_{2l}^0 + \frac{1}{v} (\tilde{\mu}_{1y} \eta_1'^{(l)} + \tilde{\mu}_{2y} \eta_2'^{(l)}), \quad l = 1, 2, 3, 5, \quad (3.5)$$

where the following notations are used

$$\begin{aligned} \eta_1'^{(l)} &= \frac{\beta}{\Delta} \{ (\psi_{l1} \eta_1 + \psi_{l2} \eta_2) [D(\kappa_{11} + \kappa_{12}) - (\tilde{\varphi}_2 - \beta\nu_2)(\kappa_{11}\kappa_{22} - \kappa_{12}^2)] \\ &- \delta_l [D\rho_1 - \rho_1(\beta\nu_2 \kappa_{12} + \tilde{\varphi}_2 \kappa_{22}) + \rho_2(\beta\nu_2 \kappa_{11} + \tilde{\varphi}_2 \kappa_{12})] \}, \\ \eta_2'^{(l)} &= \frac{\beta}{\Delta} \{ (\psi_{l2} \eta_1 + \psi_{l1} \eta_2) [D(\kappa_{22} + \kappa_{12}) - (\tilde{\varphi}_1 - \beta\nu_2)(\kappa_{11}\kappa_{22} - \kappa_{12}^2)] \\ &- \delta_l [D\rho_2 + \rho_1(\beta\nu_2 \kappa_{22} + \tilde{\varphi}_1 \kappa_{12}) - \rho_2(\beta\nu_2 \kappa_{12} + \tilde{\varphi}_1 \kappa_{11})] \}, \\ \rho_1 &= 2a \sinh y_1 - \eta_1 [2a \cosh y_1 + 2a \cosh y_2 + 4a^2], \\ \rho_2 &= 2a \sinh y_2 - \eta_2 [2a \cosh y_1 + 2a \cosh y_2 + 4a^2]. \end{aligned}$$

The constants of piezoelectric stress are obtained by differentiating the electric field over the strains at constant polarization

$$h_{2i} = - \left(\frac{\partial E_2}{\partial \varepsilon_i} \right)_{P_2} = \frac{e_{2i}}{\chi_{22}^E}. \quad (3.6)$$

The calculations of the isothermal elastic constants at a constant field yield

$$\begin{aligned} c_{il}^E &= \left(\frac{\partial \sigma_i}{\partial \varepsilon_l} \right)_{E_2} = c_{il}^{E0} - \frac{2}{v} (\psi_{i1} \eta_1 + \psi_{i2} \eta_2 + \frac{\delta_i}{D} \varkappa_1^c \tilde{\varphi}_1 + \frac{\delta_i}{D} \varkappa_2^c \beta \nu_2) \eta_1^{(l)} \\ &\quad - \frac{2}{v} (\psi_{i1} \eta_2 + \psi_{i2} \eta_1 + \frac{\delta_i}{D} \varkappa_1^c \beta \nu_2 + \frac{\delta_i}{D} \varkappa_2^c \tilde{\varphi}_2) \eta_2^{(l)} \\ &\quad - \frac{2\beta \delta_i}{v_2 D} [\psi_{l1} (\varkappa_1^c \eta_1 + \varkappa_2^c \eta_2) + \psi_{l2} (\varkappa_2^c \eta_1 + \varkappa_1^c \eta_1)] - \frac{4\beta \delta_i \delta_l}{D} \rho^c, \end{aligned} \quad (3.7)$$

where

$$\begin{aligned} \varkappa_1^c &= \sinh(y_1 + y_2) + \sinh(y_1 - y_2) - \eta_1 [\cosh(y_1 + y_2) + \cosh(y_1 - y_2) - 2a^2], \\ \varkappa_2^c &= \sinh(y_1 + y_2) - \sinh(y_1 - y_2) - \eta_2 [\cosh(y_1 + y_2) + \cosh(y_1 - y_2) - 2a^2], \\ \rho^c &= 2a^2 + \frac{[\cosh(y_1 + y_2) + \cosh(y_1 - y_2) - 2a^2]}{D} [a \cosh y_1 + a \cosh y_2 + 2a^2]. \end{aligned}$$

The other dielectric, piezoelectric, and elastic characteristics of CsH_2PO_4 can be obtained from those found above. Thus, the isothermal coefficients of the piezoelectric strain are

$$d_{2i} = \sum_j s_{ij}^E e_{2j}, \quad i, j = 1, 2, 3, 5. \quad (3.8)$$

The matrix of the isothermal elastic compliances at a constant field s_{ij}^E is inverse to the matrix of the elastic constants c_{ij}^E

$$\widehat{C^E} = \begin{pmatrix} c_{11}^E & c_{12}^E & c_{13}^E & c_{15}^E \\ c_{12}^E & c_{22}^E & c_{23}^E & c_{25}^E \\ c_{13}^E & c_{23}^E & c_{33}^E & c_{35}^E \\ c_{15}^E & c_{25}^E & c_{35}^E & c_{55}^E \end{pmatrix}, \quad \widehat{S^E} = (\widehat{C^E})^{-1}. \quad (3.9)$$

The isothermal constants of the piezoelectric strain are

$$g_{2i} = \sum_j s_{ij}^E h_{2j}. \quad (3.10)$$

The molar heat capacity of the proton subsystem of CDP at constant pressure can be found by numerically differentiating the thermodynamic potential:

$$\Delta C_p = - \frac{N_A T}{4} \left(\frac{\partial^2 g}{\partial T^2} \right)_{\sigma_j}. \quad (3.11)$$

where N_A is the Avogadro constant.

IV. COMPARISON OF THE THEORETICAL RESULTS WITH THE EXPERIMENTAL DATA. DISCUSSION

The theory parameters are determined from the condition of agreement of the calculated characteristics with experimental data for the temperature dependences of spontaneous polarization $P_2(T)$ and dielectric permittivity $\varepsilon_{22}(T)$ at different values of hydrostatic pressure [6], spontaneous strains ε_j [20], molar heat capacity [24], and elastic constants [25]; as well as with the results of the ab-initio calculations of the lattice contributions to the molar heat capacity [16] and dielectric permittivity [17].

The parameters of short-range interactions w_0 and long-range interactions ν_1^0 ("intra-sublattice"), ν_2^0 ("inter-sublattice") mainly determine the phase transition temperature from the paraelectric to the ferroelectric phase in the absence of external pressure and field; the order of the phase transition, and the shape of spontaneous polarization. Their optimum values are $w_0/k_B = 650$ K, $\nu_1^0/k_B = 1.50$ K, $\nu_2^0/k_B = 0.23$ K.

To determine the deformational potentials δ_j [see (2.2)] and ψ_{j1} (2.9), ψ_{j2} (2.10), it is necessary to use experimental data for the shift of the phase transition temperature under hydrostatic and uniaxial pressures, as well as the data for the temperature dependences of spontaneous strains ε_j , piezoelectric coefficients, and elastic constants. Unfortunately, the only available data are those for the spontaneous strains and hydrostatic pressure effect on the dielectric characteristics. As a result, experimental data for the strains and dielectric characteristics can be described using many different combinations of the parameters ψ_{j1} , ψ_{j2} . Therefore, for the sake of simplicity, we chose ψ_{j2} to be proporti-

onal to ψ_{j1} . The optimum values of the deformational potentials were determined in [23]. Their values are $\delta_1/k_B = 1214$ K, $\delta_2/k_B = 454$ K, $\delta_3/k_B = 1728$ K, $\delta_5/k_B = 1214$ K, $\delta_5/k_B = -13$ K; $\psi_{11}/k_B = 92.2$ K, $\psi_{21}/k_B = 23.2$ K, $\psi_{31}/k_B = 139.7$ K, $\psi_{51}/k_B = 5.5$ K; $\psi_{j2} = \frac{1}{3}\psi_{j1}$.

The effective dipole moment in the paraelectric phase is found by fitting the calculated curve $\varepsilon_{22}(T)$ to the experimental data. We consider it to be dependent on the value of hydrostatic pressure p , that is, $\mu_y = \mu_y^0(1 - k_p p)$, where $\mu_y^0 = 2.63 \cdot 10^{-18}$ esu-cm, $k_p = 0.4 \cdot 10^{-10}$ cm²/dyn. The correction to effective dipole moment $\mu' = -0.43 \cdot 10^{-18}$ esu-cm is found by fitting the calculated saturation polarization to the experimental data.

The “seed” dielectric susceptibility χ_{22}^{E0} , coefficients of piezoelectric stress e_{2j}^0 , and elastic constants c_{ij}^{E0} are found by fitting to the experimental data at

temperatures far from the phase transition temperature T_c . Their values are as follows $\chi_{22}^{E0} = 0.443$ [17]; $e_{2j}^0 = 0 \frac{\text{esu}}{\text{cm}^2}$; $c_{11}^{0E} = 28,83 \cdot 10^{10} \frac{\text{dyn}}{\text{cm}^2}$, $c_{12}^{E0} = 11,4 \cdot 10^{10} \frac{\text{dyn}}{\text{cm}^2}$, $c_{13}^{E0} = 42,87 \cdot 10^{10} \frac{\text{dyn}}{\text{cm}^2}$, $c_{22}^{E0} = 26,67 \cdot 10^{10} \frac{\text{dyn}}{\text{cm}^2}$, $c_{23}^{E0} = 14,5 \cdot 10^{10} \frac{\text{dyn}}{\text{cm}^2}$, $c_{33}^{E0} = 65,45 \cdot 10^{10} \frac{\text{dyn}}{\text{cm}^2}$, $c_{15}^{E0} = 5,13 \cdot 10^{10} \frac{\text{dyn}}{\text{cm}^2}$, $c_{25}^{E0} = 8,4 \cdot 10^{10} \frac{\text{dyn}}{\text{cm}^2}$, $c_{35}^{E0} = 7,50 \cdot 10^{10} \frac{\text{dyn}}{\text{cm}^2}$, $c_{55}^{E0} = 5,20 \cdot 10^{10} \frac{\text{dyn}}{\text{cm}^2}$.

The volume of the extended primitive cell is $v = 0.467 \cdot 10^{-21}$ cm³ [7].

Let us consider now the obtained results.

The effects of uniaxial and hydrostatic pressure are determined, mainly, by the pressure-induced behavior of the lattice strains ε_j . The temperature dependences of the strains at ambient pressure and in presence of uniaxial pressures are shown in Fig. 2 and in the presence of hydrostatic pressure in Fig. 3.

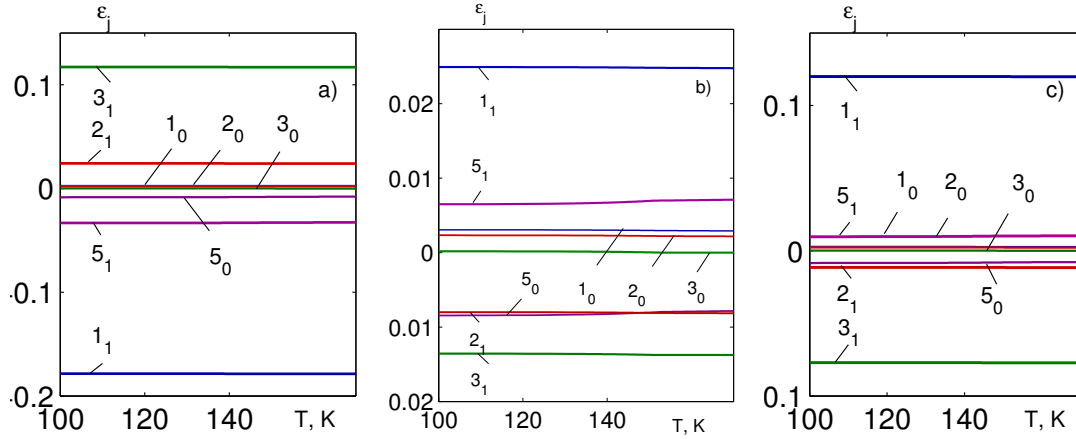


Fig. 2. The temperature dependences of the strains $\varepsilon_1 - 1$, $\varepsilon_2 - 2$, $\varepsilon_3 - 3$, $\varepsilon_5 - 5$ of CDP at different uniaxial pressures: $p_1 - a$), $p_2 - b$), $p_3 - c$). The lower index denotes the pressure values in kbar

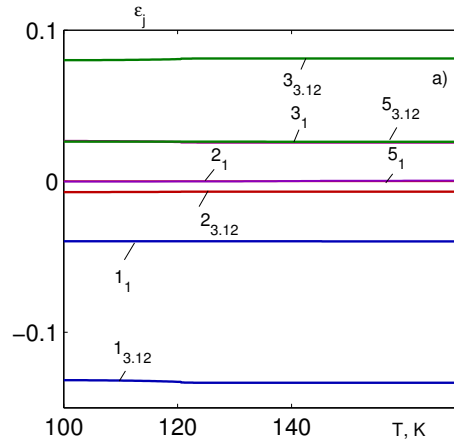


Fig. 3. The temperature dependences of the strains $\varepsilon_1 - 1$, $\varepsilon_2 - 2$, $\varepsilon_3 - 3$, $\varepsilon_5 - 5$ of CDP at different values of hydrostatic pressure p_h . The lower index denotes the pressure values in kbar

The pressure p_1 increases the negative value of the strain ε_1 and the positive value of ε_3 . The strains ε_2 , ε_5 are not changed perceptibly. The uniaxial pressure p_2 increases the negative values of the strains ε_3 and ε_2 , as well as the positive values of the strains ε_1 and ε_5 . The

pressure p_3 increases the negative values of ε_3 , ε_5 and the positive values of ε_1 and ε_5 . The magnitude of the strain ε_2 is barely changed. The pressure p_h increases the absolute values of the strains ε_1 and ε_3 and slightly increases the strain ε_5 ; the strain ε_2 is positive and hardly

changes with an increase in p_h . The lattice strains ε_j depend on pressure almost linearly, in accordance with Hooke's law.

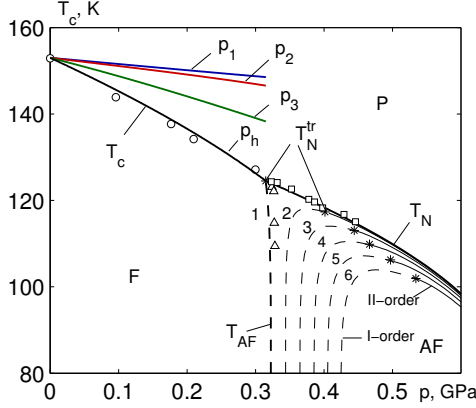


Fig. 4. The dependences of the transition temperatures of CDP on the uniaxial p_1 ; p_2 ; p_3 and hydrostatic pressures: between the paraelectric and ferroelectric phases T_c , between the paraelectric and antiferroelectric phases T_N , between the ferroelectric and antiferroelectric phases T_{AF} at different values of the electric field E_2 (MV/m): 0.0 – 1, 0.1 – 2, 0.2 – 3, 0.3 – 4, 0.4 – 5, 0.5 – 6. Symbols are the experimental data of [5]. The tricritical points T_N^{tr} (denoted by *) separate the curves of the first (dashed lines) and the second (solid lines) order phase transition

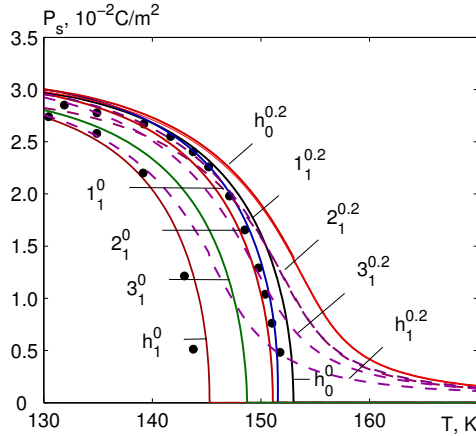


Fig. 5. The temperature dependence of the spontaneous polarization P_s of the CDP crystal at different values of uniaxial pressures ($p_1 - 1$; $p_2 - 2$; $p_3 - 3$), hydrostatic pressure (p_h), and electric field E_2 . The upper index denotes the field value in MV/m, the lower index denotes the pressure in the units of 0.1 GPa. Dots (•) are the experimental data of [5]

External pressures weaken the interactions between the pseudospins. The interaction parameters w , ν_1 , ν_2 decrease linearly with an increase in pressures. As a result, the transition temperature T_c decreases (Fig. 4). From Fig. 4 it is seen that at low pressures the change in the Curie temperature under hydrostatic pressure is approximately equal to the sum of changes in the Curie temperature under uniaxial pressures.

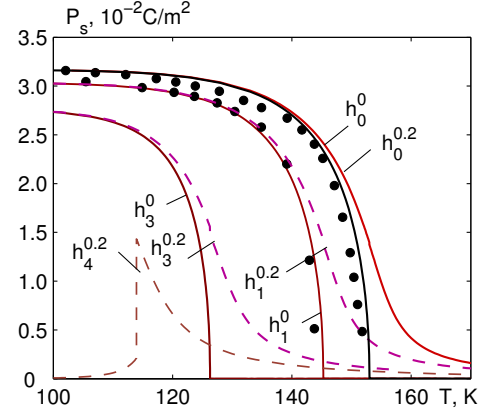


Fig. 6. The temperature dependence of the spontaneous polarization P_s of the CDP crystal at different values of hydrostatic pressure (p_h) and electric field E_2 . The upper index denotes the field value in MV/m, the lower index denotes the pressure in the units of 0.1 GPa. Dots (•) are the experimental data of [5]

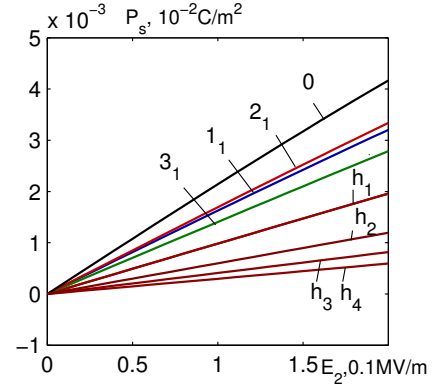


Fig. 7. Dependences of the spontaneous polarization of CDP on the electric field E_2 at different values of uniaxial pressures ($p_1 - 1$; $p_2 - 2$; $p_3 - 3$) and hydrostatic pressure (h_1, h_2, h_3, h_4). The lower index denotes the pressure in the units of 0.1 GPa

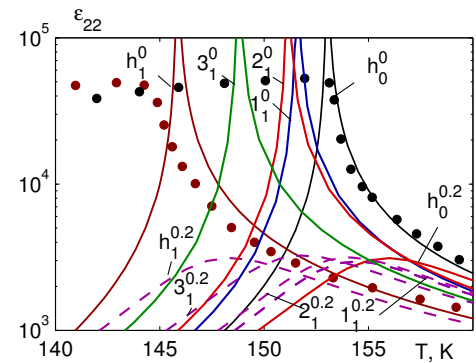


Fig. 8. The temperature dependence of the longitudinal dielectric permittivity ε_{22} of CDP at different values of uniaxial pressures ($p_1 - 1$; $p_2 - 2$; $p_3 - 3$), hydrostatic pressure (p_h), and electric field E_2 . The upper index denotes the field value in MV/m, the lower index denotes the pressure in the units of 0.1 GPa. Dots (•) are the experimental data of [5]

Since the transition temperature T_c is lowered down by the pressures, the temperature curves of the spontaneous polarization P_s (Figs. 5, 6), longitudinal dielectric permittivity ε_{22} (Figs. 8, 9), piezomoduli e_{21} , h_{21} (Figs. 11-14), elastic constant c_{11} (Figs. 16, 17), and pseudospin contribution to the heat capacity ΔC (Figs. 18, 19) all shift to lower temperatures.

In Fig. 5, we plot the temperature dependences of the

spontaneous polarization P_s of CDP at different values of the uniaxial pressures (p_1 ; p_2 ; p_3), hydrostatic pressure p_h , and electric field E_2 . The temperature dependence of the spontaneous polarization P_s at different values of hydrostatic pressure (p_h) and electric field E_2 is shown in Fig. 6, whereas the dependences of P_s on the electric field E_2 at different values of uniaxial and hydrostatic pressures are shown in Fig. 7.

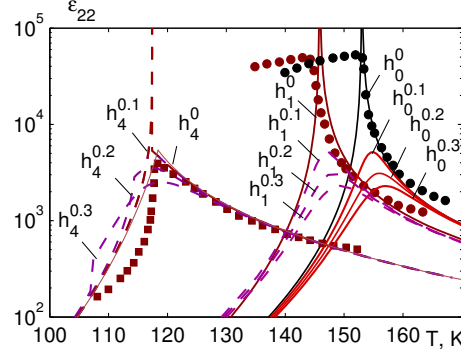


Fig. 9. The temperature dependence of the longitudinal dielectric permittivity ε_{22} of CDP at different values of hydrostatic pressure (p_h) and electric field E_2 . The upper index denotes the field value in MV/m, the lower index denotes the pressure in the units of 0.1 GPa. Dots (•) are the experimental data of [5]

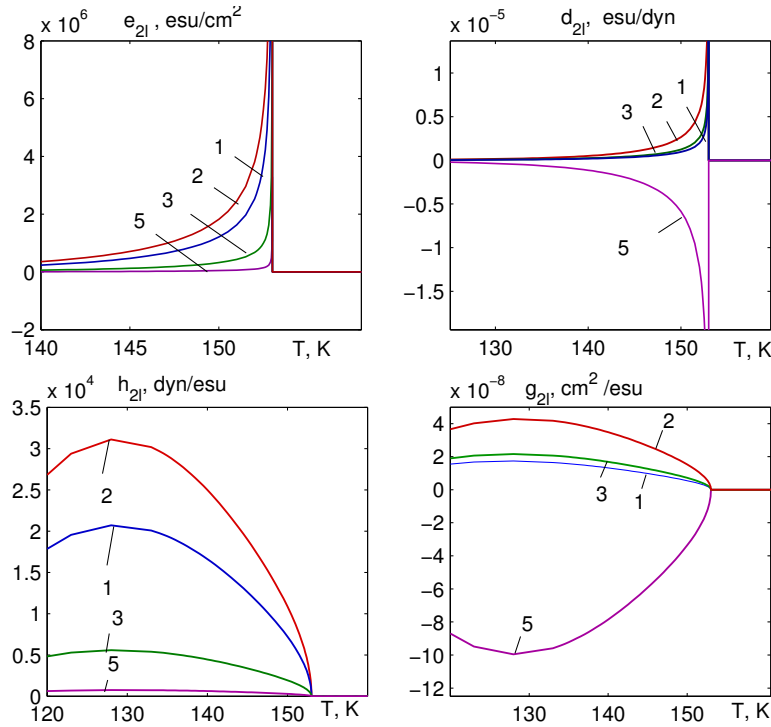


Fig. 10. The temperature dependences of the coefficients of piezoelectric stress $e_{21} - 1$, $e_{22} - 2$, $e_{23} - 3$, $e_{25} - 4$, coefficients of piezoelectric strain $d_{21} - 1$, $d_{22} - 2$, $d_{23} - 3$, $d_{25} - 4$, constants of piezoelectric stress $h_{21} - 1$, $h_{22} - 2$, $h_{23} - 3$, $h_{25} - 4$, and constants of piezoelectric strain $g_{21} - 1$, $g_{22} - 2$, $g_{23} - 3$, $g_{25} - 4$ of the CDP crystal

At low pressures, the spontaneous polarization monotonically and continuously decreases with an increase in temperature and vanishes at T_c . The phase transition at T_c is still of the second order.

The application of the external field E_2 smears out the polarization curves, and the phase transition in CDP disappears as such.

The electric field E_2 decreases the polarization. The largest decrease is observed when the electric field and hydrostatic pressure are applied simultaneously.

The longitudinal dielectric permittivity ε_{22} diverges at T_c (figs. 8, 9). In the presence of the electric field E_2 , the permittivity ε_{22} has a jump at T_N instead of a cusp (Fig. 9).

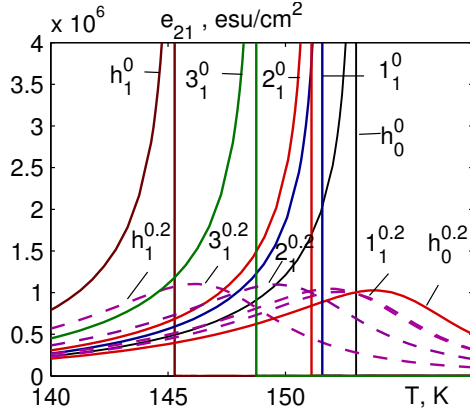


Fig. 11. The temperature dependences of the coefficient of piezoelectric stress e_{21} at different values of uniaxial pressures ($p_1 - 1$; $p_2 - 2$; $p_3 - 3$), hydrostatic pressure (p_h), and electric field E_2 . The upper index denotes the field value in MV/m, the lower index denotes the pressure in the units of 0.1 GPa

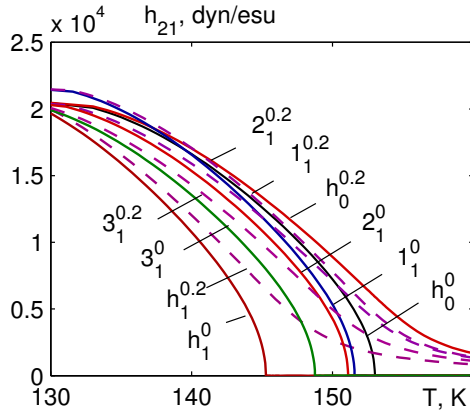


Fig. 12. The temperature dependences of the constant of piezoelectric stress h_{21} at different values of uniaxial pressures ($p_1 - 1$; $p_2 - 2$; $p_3 - 3$), hydrostatic pressure (p_h), and electric field E_2 . The upper index denotes the field value in MV/m, the lower index denotes the pressure in the units of 0.1 GPa

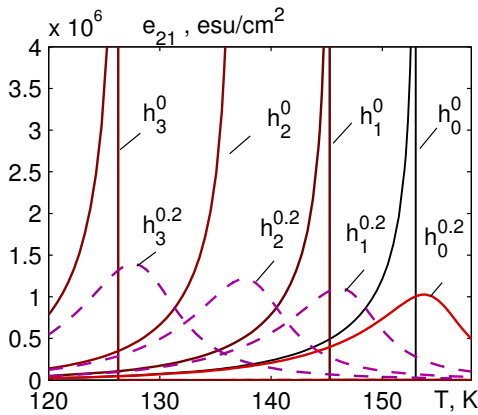


Fig. 13. The temperature dependences of the coefficient of piezoelectric stress e_{21} at different values of hydrostatic pressure (p_h) and electric field E_2 . The upper index denotes the field value in MV/m, the lower index denotes the pressure in the units of 0.1 GPa

In the presence of the electric field E_2 the permittivity ε_{22} remains finite and has maxima, whose magnitudes decrease with an increase in the field, and which positions shift to higher temperatures.

The theoretical results agree quantitatively well with the experimental data of [5] for the case of hydrostatic pressure p_h . It should be mentioned that the theory is developed for a single-domain crystal and does not take into account the reorientation of domain walls, which gives an essential contribution to the experimentally measured permittivity. That is why the calculated permittivity ε_{22} in the ferroelectric phase does not agree with the experimental data.

The piezoelectric coefficients e_{2l} and d_{2l} increase with temperature and diverge at T_c (Fig. 10), whereas the constants h_{2l} and g_{2l} have rounded maxima and approach zero at T_c .

In Figs. 11, 12 the temperature curves of the piezoelectric stress coefficient e_{21} and constant h_{21} of the CDP crystal are shown at different values of uniaxial pressures ($p_1; p_2; p_3$), hydrostatic pressure p_h , and electric field E_2 . Their temperature curves at different values of hydrostatic pressure (p_h) and electric field E_2 are presented in Figs. 13, 14.

Hydrostatic pressure p_h increases the maximum value of the piezoelectric stress constant h_{21} ; the influence of the electric field E_2 at lower temperatures is weak. The field E_2 smears out the curves of the piezoelectric stress constant h_{21} .

The field E_2 applied to the CDP crystal decreases the maximum values of the coefficient of piezoelectric stress e_{21} and shifts them to higher temperatures.

The elastic constants c_{ij} of CDP are virtually temperature independent, except for small jumps at T_c (Fig. 15).

In Fig. 16, we depict the temperature dependences of the elastic constant c_{11} of CDP at different values of the uniaxial pressures ($p_1; p_2; p_3$), hydrostatic pressure p_h , and electric field E_2 . Its temperature dependences at different values of hydrostatic pressures (p_h) and electric field E_2 are presented in Fig. 17.

In the presence of the pressures, the jump of the elastic constant c_{11} deepens. The effect of the uniaxial pressure p_3 is the strongest. Hydrostatic pressure p_h lowers down c_{11} . The electric field E_2 smears out the curves of the elastic constant c_{11} ; its minimum values increase with an increase in pressures. Outside the vicinity of the transition temperature, the field E_2 does not affect the elastic constants c_{ij}^E .

The temperature curves of the pseudospin contribution to the heat capacity ΔC_p of CDP in presence of the uniaxial pressures p_i exhibit jumps at the phase transition temperature and shift to lower temperatures (Fig. 18). The magnitude of the jumps is slightly decreased by the pressures p_i .

The temperatures dependences of ΔC_p remain qualitatively unchanged by hydrostatic pressure (Fig. 19). Positions of the heat capacity maximum shift to lower temperatures, whereas the magnitude of ΔC_{p_h} decrease, with an increase in hydrostatic pressure.

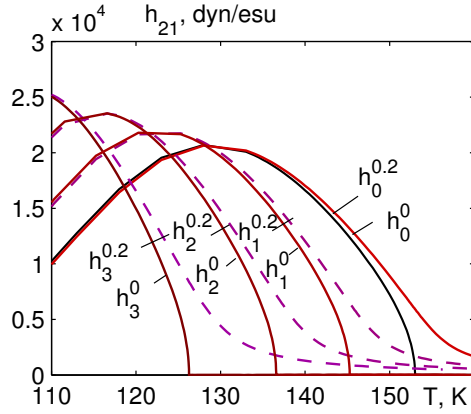


Fig. 14. The temperature dependences of the constant of piezoelectric stress h_{21} at different values of hydrostatic pressure (p_h) and electric field E_2 . The upper index denotes the field value in MV/m, the lower index denotes the pressure in the units of 0.1 GPa

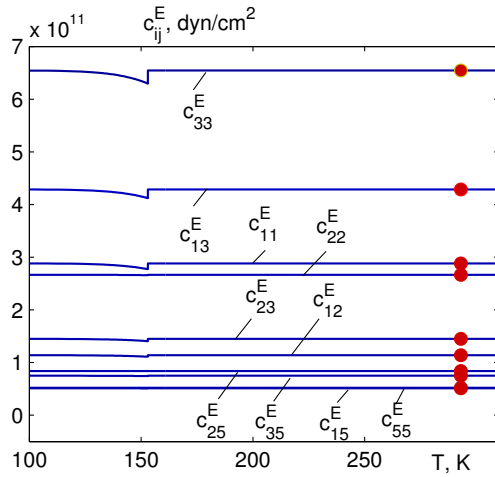


Fig. 15. The temperature dependences of the elastic constants c_{ij} of CDP. Dots (•) are the experimental data of [25]

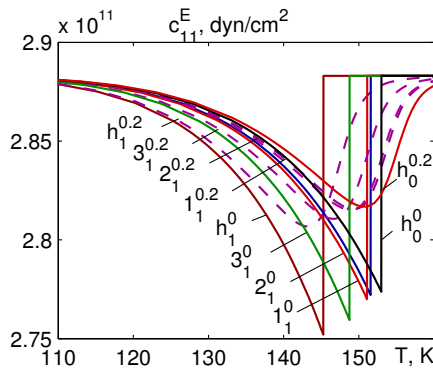


Fig. 16. The temperature dependences of the elastic constant c_{11} at different values of uniaxial pressures ($p_1 - 1$; $p_2 - 2$; $p_3 - 3$), hydrostatic pressure (p_h), and electric field E_2 . The upper index denotes the field value in MV/m, the lower index denotes the pressure in the units of 0.1 GPa

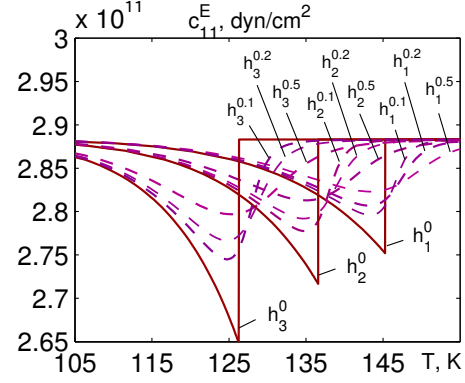


Fig. 17. The temperature dependences of the elastic constant c_{11} at different values of hydrostatic pressure (p_h) and electric field E_2 . The upper index denotes the field value in MV/m, the lower index denotes the pressure in the units of 0.1 GPa

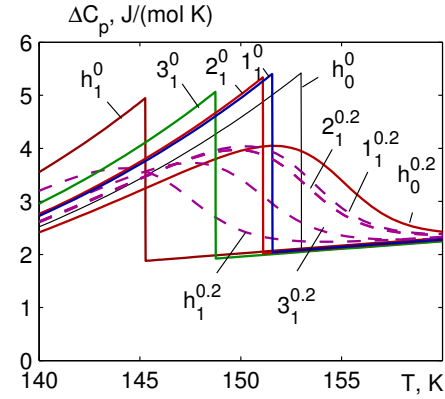


Fig. 18. The temperature dependences of the proton contribution to molar heat capacity at different values of uniaxial pressures ($p_1 - 1$; $p_2 - 2$; $p_3 - 3$), hydrostatic pressure (p_h), and electric field E_2 . The upper index denotes the field value in MV/m, the lower index denotes the pressure in the units of 0.1 GPa

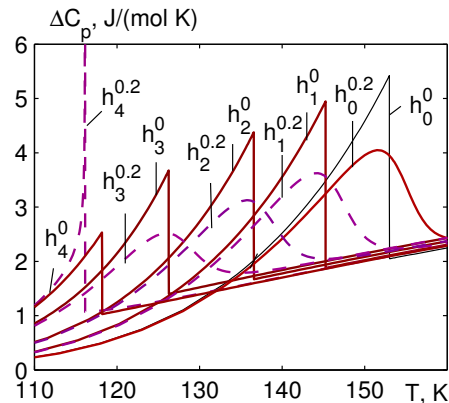


Fig. 19. The temperature dependences of the proton contribution to molar heat capacity at different values of hydrostatic pressure (p_h) and electric field E_2 . The upper index denotes the field value in MV/m, the lower index denotes the pressure in the units of 0.1 GPa

In Figs. 18, 19, we plot the temperature dependences of the pseudospin contributions to the heat capacity ΔC of CDP in the presence of the electric field E_2 , as well as of the pressures and the field E_2 simultaneously. The jump of ΔC is smeared out by the field E_2 , and its maximum value is decreased. In the antiferroelectric phase, the molar heat capacity is also reduced by the field.

V. CONCLUSIONS

In the present work, within the framework of the modified proton ordering model for the quasi-one-dimensional CsH_2PO_4 ferroelectric with hydrogen bonds, which takes into account the contributions to the energy of the proton subsystem that are linear in the lattice strains ε_1 , ε_2 , ε_3 , and ε_5 , within the two-particle cluster approximation, we studied the influence of hydrostatic and uniaxi-

al pressures and the longitudinal electric field E_2 on the phase transition and physical characteristics of this ferroelectric. It has been established that the uniaxial and hydrostatic pressure change the lattice strains ε_i , ε_5 , thereby changing the transition temperature and other characteristics of the crystal.

Since the transition temperatures T_c are decreased by the pressures, the temperature curves of the spontaneous polarization P_s , longitudinal dielectric permittivity ε_{22} , piezomoduli e_{21} , d_{21} , h_{21} , g_{21} , elastic constant c_{11} , and pseudospin contribution to the heat capacity ΔC shift to lower temperatures under pressures.

At pressures $p < p_c$ the external field smears out the phase transition. At $p > p_c$ the field lowers down the transition temperature T_N and discontinuously increases the permittivity ε_{22} , elastic constant c_{11} , and pseudospin contribution to the heat capacity ΔC in the antiferroelectric phase at $E_2 = 0.1$ MV/m.

-
- [1] H. Matsunaga, K. Itoh, E. Nakamura, J. Phys. Soc. Jpn. **48**, 2011 (1980); <https://doi.org/10.1143/JPSJ.48.2011>.
 - [2] K. Itoh, T. Hagiwara, E. Nakamura, J. Phys. Soc. Jpn. **52**, 2626 (1983); <https://doi.org/10.1143/JPSJ.52.2626>.
 - [3] Y. Iwata, N. Koyano, I. Shibuya, J. Phys. Soc. Jpn. **49**, 304 (1980); <https://doi.org/10.1143/JPSJ.49.304>.
 - [4] Y. Iwata *et al.*, J. Phys. Soc. Jpn. **63**, 4044 (1994); <https://doi.org/10.1143/JPSJ.63.4044>.
 - [5] N. Yasuda *et al.*, Phys. Rev. Lett. **41**, 1311 (1978); <https://doi.org/10.1103/PhysRevLett.41.1311>.
 - [6] N. Yasuda, S. Fujimoto, M. Okamoto, H. Shimizu, K. Yoshino, Y. Phys. Rev. B **20**, 2755 (1979); <https://doi.org/10.1103/PhysRevB.20.2755>.
 - [7] P. J. Schuele, R. A. Thomas, Jap. J. Appl. Phys. **24**, 935 (1985); <https://doi.org/10.7567/JJAPS.24S2.935>.
 - [8] P. J. Schuele, V. H. Schmidt, Phys. Rev. B **39**, 2549, (1989); <https://doi.org/10.1103/PhysRevB.39.2549>.
 - [9] Yu. Kobayashi *et al.*, Ferroelectrics **285**, 83 (2003); <https://doi.org/10.1080/00150190390205924>.
 - [10] K. Gesi, K. Ozawa, Jpn. J. Appl. Phys. **17**, 435 (1978); <https://doi.org/10.1143/JJAP.17.435>.
 - [11] N. B. Brandt, S. G. Zhukov, V. A. Kulbachinskii, P. S. Smirnov, B. A. Strukov, Fiz. Tverd. Tela **28**, 3159 (1986).
 - [12] E. Magome, S. Tomiaka, Y. Tao, M. Komukae, J. Phys. Soc. Jpn. **79**, 025002 (2010); <https://doi.org/10.1143/JPSJ.79.025002>.
 - [13] Ya. Shchur, Phys. Rev. B **74**, 054301 (2006); <https://doi.org/10.1103/PhysRevB.74.054301>.
 - [14] Ya. Shchur, Phys. Status Solidi B **244**, 569 (2007); <https://doi.org/10.1002/pssb.200642176>.
 - [15] J. Lasave, P. Abufager, S. Koval, Phys. Rev. B **93**, 134112 (2016); <https://doi.org/10.1103/PhysRevB.93.134112>.
 - [16] Ya. Shchur, T. Bryk, I. Klevets, A.V. Kityk, Comput. Mater. Sci. **111**, 301 (2016); <https://doi.org/10.1016/j.commatsci.2015.09.014>.
 - [17] B. Van Troeye *et al.*, Phys. Rev. B **95**, 024112 (2017); <https://doi.org/10.1103/PhysRevB.95.024112>.
 - [18] R. Blinc, F. C. SaBaretto, J. Chem. Phys. **72**, 6031 (1988); <https://doi.org/10.1063/1.439058>.
 - [19] I. V. Stasyuk *et al.*, preprint ICMP-91-4R (Lviv, 1991).
 - [20] K. Deguchi, E. Okaue, S. Ushio, E. Nakamura, K. Abe, J. Phys. Soc. Jpn. **53**, 3074 (1984); <https://doi.org/10.1143/JPSJ.53.3074>.
 - [21] R. R. Levitskii, I. R. Zachek, A. S. Vdovych, Phys. Chem. Solid State **13**, 40 (2012).
 - [22] R. R. Levitskii, I. R. Zachek, A. S. Vdovych, J. Phys. Stud. **16**, 4702 (2012); <https://doi.org/10.30970/jps.16.4702>.
 - [23] A. S. Vdovych, I. R. Zachek, R. R. Levitskii, Condens. Matter Phys. **23**, 33702 (2020); <https://doi.org/10.5488/CMP.23.33702>.
 - [24] K. Imai, J. Phys. Soc. Jpn. **52**, 3960 (1983); <https://doi.org/10.1143/JPSJ.52.3960>.
 - [25] S. Praver, T. F. Smith, T. R. Finlayson, Aust. J. Phys. **38** 63 (1985); <https://doi.org/10.1071/PH850063>.
 - [26] Y. Uesu, J. Kobayashi, Phys. Status Solidi A **34**, 475 (1976); <https://doi.org/10.1002/pssa.2210340207>.
 - [27] R. J. Nelmess, R. N. P. Choudhary, Solid State Commun. **26**, 823 (1978); [https://doi.org/10.1016/0038-1098\(78\)90751-2](https://doi.org/10.1016/0038-1098(78)90751-2).
 - [28] B. C. Fraser, D. Semmingsen, W. D. Ellenson, D. Shirane, Phys. Rev. B **20**, 2745 (1979); <https://doi.org/10.1103/PhysRevB.20.2745>.

**ВПЛИВ ОДНОВІСНИХ ТА ГІДРОСТАТИЧНОГО ТИСКІВ І ПОЗДОВЖНЬОГО
ЕЛЕКТРИЧНОГО ПОЛЯ НА ФАЗОВІ ПЕРЕХОДИ ТА ТЕРМОДИНАМІЧНІ ХАРАКТЕРИСТИКИ
КВАЗІОДНОВИМІРНОГО СЕГНЕТОЕЛЕКТРИКА CsH_2PO_4**

А. С. Вдович¹, Р. Р. Левицький¹, І. Р. Зачек², А. П. Моїна¹

¹*Інститут фізики конденсованих систем НАН України,
вул. Свенцицького, 1, Львів, 79011, Україна,*

²*Національний університет "Львівська політехніка",
вул. С. Бандери 12, 79013, Львів, Україна*

Квазіодновимірний кристал із водневими зв'язками CsH_2PO_4 є сегнетоелектриком типу лад-безлад. Фазовий перехід із високотемпературної парафази в низькотемпературну сегнетофазу пов'язаний з упорядкуванням протонів на водневих зв'язках.

Запропоновано модифіковану двопідґраткову псевдоспінову модель сегнетоелектрика CsH_2PO_4 , у якій положенням протонів приписано ефективні дипольні моменти та псевдоспіни, а кристал розглядається як система взаємодійних псевдоспінів. Ця модель урахує лінійні за деформаціями ґратки ϵ_1 , ϵ_2 , ϵ_3 і ϵ_5 внески в енергію протонної підсистеми, а також залежність ефективних дипольних моментів псевдоспінів від параметрів упорядкування, що дозволяє узгодити ефективні дипольні моменти в сегнето- і парафазі.

У межах цієї моделі в наближенні двочастинкового кластера за короткосяжними й середнього поля за далекосяжними взаємодіями досліджено поведінку спонтанної поляризації, поздовжньої діелектричної проникності, п'єзоелектричних, пружних характеристик і молярної теплоємності. Вивчено вплив гідростатичного та одновісних тисків, а також поздовжнього електричного поля на фазовий перехід та фізичні характеристики кристала. Отримано задовільний кількісний опис відповідних експериментальних даних.

Показано, що під дією одновісних тисків, а також гідростатичного тиску, меншого за критичний $p < p_c$, знижується температура фазового переходу пара-сегнетофаза. При цьому температурні залежності різних термодинамічних характеристик якісно подібні, як за відсутності тисків. Зовнішнє електричне поле за тисків $p < p_c$ розмиває фазовий перехід.

За гідростатичного тиску $p > p_c$ виникає перехід в антисегнетофазу. Електричне поле за $p > p_c$ знижує температуру фазового переходу пара-антисегнетофаза й збільшує проникність ϵ_{22} в антисегнетофазі. Достатньо сильне поле може змінити рід фазового переходу в точці T_N із другого на перший.

Найсильніший вплив поля на розраховані характеристики є поблизу критичного гідростатичного тиску p_c ; із пониженням температури кристал CsH_2PO_4 переходить спершу з парафази в антисегнетофазу, а за подальшого пониження температури — з антисегнетофази в сегнетофазу. Поздовжнє поле E_2 збільшує критичний гідростатичний тиск p_c у кристалі CsH_2PO_4 .

Ключові слова: сегнетоелектрики, діелектрична проникність, п'єзоелектричні коефіцієнти, вплив тиску, вплив електричного поля.